PEPT and Discrete Particle Simulation Study of Spout-Fluid Bed Regimes

J. M. Link, N. G. Deen, and J. A. M. Kuipers
Faculty of Science and Technology, University of Twente, 7500 AE Enschede, The Netherlands

X. Fan, A. Ingram, and D. J. Parker
Positron Imaging Centre, School of Physics and Astronomy, University of Birmingham, Birmingham B15 2TT, U.K.

J. Wood and J. P. K. Seville
Dept. of Chemical Engineering, University of Birmingham, Birmingham B15 2TT, U.K.

DOI 10.1002/aic.11456
Published online March 3, 2008 in Wiley InterScience (www.interscience.wiley.com).

The results of a combined experimental and simulation study on the flow regimes that can be encountered during spout-fluid bed operation are reported. A regime map for a three-dimensional (3D) spout-fluid bed was composed, employing spectral analysis of pressure drop fluctuations and fast video recordings. In addition, 3D Euler–Lagrangian computations were performed to assess the capability of the model to reproduce the experimentally observed flow regimes. Spectral analysis of pressure drop fluctuations revealed that for most investigated regimes the model is able to predict the appropriate regime. The frequency at which the largest power is found is overpredicted by the model in most cases. The remaining differences between the simulated and the experimentally observed bed behavior are most probably related to the representation of the effective fluid–particle interaction in the model, which relies on local spatial homogeneity. The simulation results were compared with velocity maps determined from particle trajectories acquired using positron emission particle tracking. The model accurately reproduces measured particle velocities, including their root mean square, for all investigated conditions and is therefore able to capture the details of the particle flow in various flow regimes. © 2008 American Institute of Chemical Engineers *AIChE J,* 54: 1189–1202, 2008
Keywords: particle technology, particulate flows, computational fluid dynamics (CFD), fluidization

Introduction

Spout-fluid beds are used for a variety of processes involving particulate solids, such as coating, drying, granulation (e.g., of fertilizer pellets), and pyrolysis. The spout-fluid bed combines a number of favorable properties of both spouted and fluidized beds, such as efficient contacting between particles and a gas and fluidization of Geldart D powders without slug formation.

Understanding of the particle behavior inside spout-fluid beds is crucial for their successful application and has a sensitive dependence upon the operating conditions. A detailed understanding of the particle behavior observed in spout-fluid

Correspondence concerning this article should be addressed to N. G. Deen at n.g.deen@utwente.nl.

Current address of J. P. K. Seville: School of Engineering, University of Warwick, Coventry CV4 7AL, U.K.

beds is lacking. Detailed hydrodynamic models can be used to obtain information on the flow regime, which is difficult, if not impossible, to obtain otherwise.

In early modeling studies (for example, Ref. 1) only the overall behavior of the bed was considered, neglecting the details of particle motion. Kawaguchi et al.[2] and Link et al.[3] used discrete particle models (DPM) to carry out detailed studies of the particle motion in, respectively, a spouted bed and a spout-fluid bed. They solved the volume-averaged Navier–Stokes equations for the gas phase, taking two-way coupling into account. Newton's laws were applied to compute the motion of each individual particle.

To be able to take full advantage of the detailed information provided by the model, its ability to predict the behavior of the particles in a real system needs to be assessed. This can be achieved by comparing the predictions of the model with the results of nonintrusive techniques for measuring the particle motion, such as positron emission particle tracking (PEPT). PEPT tracks the motion of a single activated particle in a given system over a period of time of order 1 h. Seville et al.[4] summarizes the past work on application of PEPT to the study of engineering equipment, while Stein et al.[5,6] and Hoomans et al.[7] applied PEPT to fluidized beds.

PEPT can be seen as a member of nonintrusive particle tracking techniques. The technique Computer Automated Radioactive Particle Tracking (CARPT) tracks an individual particle in a somewhat similar way to PEPT.[8,9] However, it has the disadvantage that tagging the particle with radioactive material, whilst maintaining the physical properties of the particle is very difficult. Optical techniques like particle image velocimetry[10] and particle tracking velocimetry have the disadvantage that they can only be used in systems that are optically accessible, which is clearly not the case for a fully three-dimensional (3D) spout fluidized bed.

Several papers have been published which compare the experimental and numerical results obtained in spouted beds, i.e., in the absence of background fluidization air.[2,11–14] When compared with spout fluidized beds, the dynamics of the system are considerably different. To the best of our knowledge, this is the first work that makes an extensive experimental/numerical comparison for the case of spout-fluidized beds.

The organization of this paper is as follows: a brief description of the theoretical model will be given first, followed by a description of the applied experimental techniques used. Subsequently, the experimental procedure will be briefly discussed. Then the operating conditions that facilitate the validation of the model for different regimes are presented, which are selected based on flow regime maps. Finally, the experimental and simulation results are presented and discussed.

Theoretical model

A 3D hard-sphere DPM was used to simulate the behavior of a spout-fluid bed. This model is described in detail in Link et al.[15] and is based on the model originally developed by Hoomans et al.[16] A short description of the model is given in this section.

In the hard-sphere collision model, rigid particles are assumed to interact through binary, instantaneous collisions. Particle collision dynamics are described by collision laws, which account for energy dissipation due to nonideal particle–particle and particle–wall interaction by means of the empirical coefficients of normal and tangential restitution, and the coefficient of friction. For systems that are not too dense, the hard-sphere model is considerably faster than soft-sphere models. Unlike soft-sphere models, the hard-sphere model cannot account for the possible occurrence of multiple collisions at the same instant. However, it has been shown that this does not lead to any serious discrepancies, as both models statistically give the same results for dense fluidized beds, provided that there are no stagnant zones in the bed.[16] For further details on the collision model the interested reader is referred to the work of Hoomans et al.[16]

Table 1. Particle Properties

Property	Value	Unit
Material	Glass	–
d_p	4.04 ± 0.02	mm
ρ_p	2526 ± 1	kg/m^3
u_{mf}	1.77 ± 0.03	m/s
$e_{n,\ p \leftrightarrow p}$	0.97*	–
$e_{n,\ p \leftrightarrow w,\ glass}$	0.97*	–
$e_{n,\ p \leftrightarrow w,\ polycarbonate}$	0.97*	–
$e_{n,\ p \leftrightarrow w,\ aluminum}$	0.97*	–
$\mu_{p \leftrightarrow p}$	0.10*	–
$\mu_{p \leftrightarrow w,\ glass}$	0.10*	–
$\mu_{p \leftrightarrow w,\ polycarbonate}$	0.10*	–
$\mu_{p \leftrightarrow w,\ aluminum}$	0.10*	–
$\beta_{0,\ p \leftrightarrow p}$	0.33*	–
$\beta_{0,\ p \leftrightarrow w,\ glass}$	0.33*	–
$\beta_{0,\ p \leftrightarrow w,\ polycarbonate}$	0.33*	–
$\beta_{0,\ p \leftrightarrow w,\ aluminum}$	0.33*	–

*Estimated values based on the experimentally determined collision properties of 2.5 particles; see Kharaz et al.[19]

The particle collision parameters play an important role in the overall bed behavior as reported by Goldschmidt et al.[18] For this reason the collision parameters, for both particle-particle and particle-wall collisions, were accurately determined by separate impact experiments and subsequently used in the simulations. An overview of the particle properties including the collision parameters is given in Table 1.

The motion of each individual particle present in the system is calculated from the Newtonian equation of motion:

$$m_p \frac{d\mathbf{v}_p}{dt} = -V_p \nabla p + \frac{V_p \beta}{\varepsilon_p}(\mathbf{u}_f - \mathbf{v}_p) + m_p \mathbf{g} \tag{1}$$

where β represents the interphase momentum transfer coefficient due to drag, which is calculated using a drag relation proposed by Koch and Hill[20] based on lattice-Boltzmann simulations:

$$\beta_{\text{Koch\&Hill}} = \frac{18\mu_f \varepsilon_f^2 \varepsilon_p}{d_p^2}(F_0(\varepsilon_p) + \tfrac{1}{2}F_3(\varepsilon_p) Re_p) \tag{2}$$

where $\varepsilon_f = 1 - \varepsilon_p$ and Re_p is given by

$$Re_p = \frac{\varepsilon_f \rho_f |\mathbf{u}_f - \mathbf{v}_p| d_p}{\mu_f} \tag{3}$$

and with

$$F_0(\varepsilon_p) = \begin{cases} \dfrac{1 + 3\sqrt{\frac{\varepsilon_p}{2}} + \frac{135}{64}\varepsilon_p \ln(\varepsilon_p) + 16.14\varepsilon_p}{1 + 0.681\varepsilon_p - 8.48\varepsilon_p^2 + 8.16\varepsilon_p^3} & \text{if } \varepsilon_p < 0.4 \\ \dfrac{10\varepsilon_p}{\varepsilon_f^3} & \text{if } \varepsilon_p \geq 0.4 \end{cases} \quad (4)$$

$$F_3(\varepsilon_p) = 0.0673 + 0.212\varepsilon_p + \frac{0.0232}{\varepsilon_f^5} \quad (5)$$

The gas phase flow field is computed from the volume-averaged Navier–Stokes equations given by

$$\frac{\partial}{\partial t}(\varepsilon_f \rho_f) + \nabla \cdot (\varepsilon_f \rho_f \mathbf{u}_f) = 0 \quad (6)$$

$$\frac{\partial}{\partial t}(\varepsilon_f \rho_f \mathbf{u}_f) + \nabla \cdot (\varepsilon_f \rho_f \mathbf{u}_f \mathbf{u}_f) = -\varepsilon_f \nabla p - \nabla \cdot (\varepsilon_f \tau_f) - \mathbf{S}_p + \varepsilon_f \rho_f \mathbf{g} \quad (7)$$

where the fluid density, ρ_f, is determined using the ideal gas law and the viscous stress tensor, τ_f, is assumed to obey the general form for a Newtonian fluid:[21]

$$\tau_f = -\left[\left(\lambda_f - \frac{2}{3}\mu_f\right)(\nabla \cdot \mathbf{u}_f)\mathbf{I} + \mu_f\left((\nabla \mathbf{u}_f) + (\nabla \mathbf{u}_f)^T\right)\right] \quad (8)$$

Two-way coupling is achieved via the sink term, $\mathbf{S}_p$, which is computed from

$$\mathbf{S}_p = \frac{1}{V_{cell}} \sum_{\forall i \in cell} \frac{V_i \beta}{\varepsilon_p}(\mathbf{u}_f - \mathbf{v}_i) D(\mathbf{r} - \mathbf{r}_i) \quad (9)$$

The distribution function, D, distributes the reaction force acting on the gas phase to the velocity nodes in the (staggered) Eulerian grid.

Experimental technique

PEPT[4] takes advantage of a particular class of radioisotopes, which decay through the emission of positrons. When the positrons encounter electrons, they are annihilated, each annihilation converting matter into two back-to-back 511 keV gamma rays. These gamma rays are simultaneously detected by a pair of detectors. The position of the particle emitting the positrons is reconstructed by calculating the point of intersection of several pairs of gamma rays, which is illustrated in Figure 1. This technique was used to determine the solids motion in the spout-fluid bed, as discussed below.

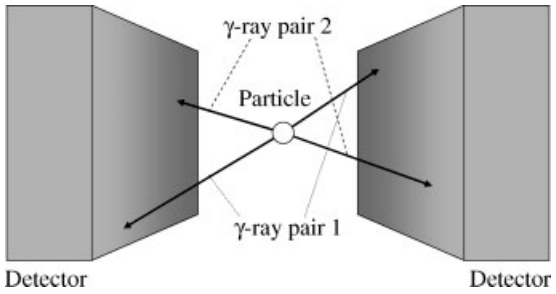

Figure 1. Illustration of the detection of a particle based on successive back-to-back γ-ray pairs emerging from a particle.

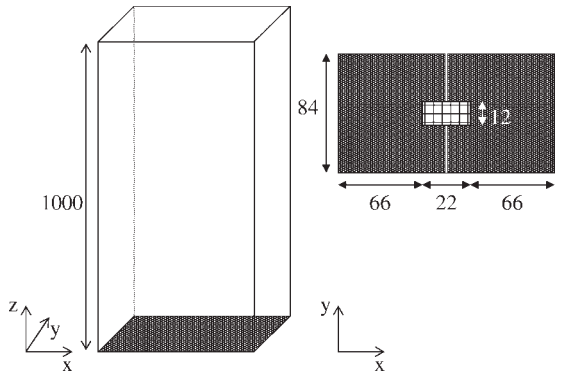

Figure 2. Schematic representation of the geometry of the 3D spout-fluid bed; dimensions are given in millimeters.

Zhang and Tang[22] and Link et al.[15] showed that valuable information about the dynamics of the particle behavior inside a spout-fluid bed can be obtained from spectral analysis of the pressure drop fluctuations. The flow regime can be determined based on the characteristic frequency peaks that are present in the frequency spectrum resulting from the Fourier transformation.

The 3D spout-fluid bed setup used in this work consists of the gas-fluidized bed schematically represented in Figure 2. The side walls of the bed are made of aluminum, whereas the front and back walls are made of polycarbonate. Pressurized air was fed to the bed through three separate sections, to ensure uniform gas distribution. A 2-mm-thick porous plate with an average pore size of 100 μm provided a homogeneous gas distribution over the two fluidization sections. Figure 2 shows that the bed contains a spout section, which is covered by a 0.5-mm metal gauze and located on the border between the two fluidization sections at the geometrical center of the bottom plate. A monodisperse size distribution consisting of 4.48×10^4 particles was used.

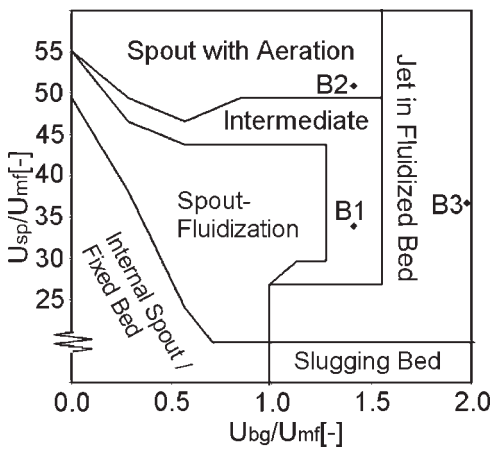

Figure 3. Flow regime map of the investigated 3D spout-fluid bed.

Table 2. Test Cases for the 3D Spout-Fluid Bed

Case	Flow Regime	u_{bg} (m/s)	u_{bg}/u_{mf} (−)	u_{sp} (m/s)	u_{sp}/u_{mf} (−)	u_{sup} (m/s)	u_{sup}/u_{mf} (−)	t_{sim} (s)	t_{PEPT} (s)	t_{pdf} (s)	
										UK	NL
B1	Intermediate/spout-fluidization	2.5	1.4	60	34	3.7	2.1	20	3600	119	51
B2	Spouting-with-aeration	2.5	1.4	90	51	4.3	2.4	20	3600	119	68
B3	Jet-in-fluidized-bed	3.5	2.0	65	37	4.8	2.7	20	3600	120	60

The properties of the particles that were used are given in Table 1.

During all experiments, the fluctuations in the bed pressure drop (excluding the gas distributor) were recorded using a high-frequency pressure probe (Kulite XT-190M-0.35BAR VG) at a frequency of 100 Hz. The pressure probe was positioned in the middle of the back wall of the bed about 0.01 m above the porous plate. The pressure drop fluctuations were recorded over a period of at least 1 min.

During the PEPT measurements, the bed was placed between the detectors, covering a height of 0.47 m. Depending on the amount of radiation emitted by the single tracer particle, the space between the detectors and the bed was varied. The tracer particle was produced by exposing one of the particles used in the experiments to a ^{3}He beam generated by a cyclotron, so as to produce the positron emitter ^{18}F from some of the ^{16}O in the glass. The position of the tracer particle was recorded over a period of 1 h at a frequency ranging from 100 to 300 Hz depending on the amount of radiation emitted by the single tracer particle and the location of the detectors. The data produced from the PEPT measurements consist of the particle positions in three dimensions as a function of time. Depending on the position with respect to the detectors, the output contains a variable amount of noise. The noise is most severe in the horizontal plane near the bottom of the bed, which is close to the edge of the PEPT detectors. Near the bottom of the detectors the differences in the slopes of the intersecting γ-ray pairs in the x and y direction are small. Therefore, the accuracy of the point of intersection, representing the location of the tracer particle, in those directions will be reduced, increasing the amount of noise. To suppress the noise, a cubic smoothing spline was applied to the PEPT output data. Occasionally, the tracer particle left the detectable range, because the PEPT detectors only covered the lowest 0.47 m of the bed. In that case, the readings directly before exit and after return of the particle were discarded.

To diminish the effect of the remaining noise on the time-averaged velocities, all velocities are calculated using the average velocity over six subsequent particle locations. The velocity is subsequently assigned to the cell containing the average over six particle locations.

Flow regime map and case selection

The objective of this work is to study the behavior of a 3D spout-fluid bed and, more importantly, to assess the capability of the model to predict the experimentally observed behavior. To ensure that the main flow regimes encountered in a spout-fluid bed were considered, a flow regime map has been assembled from which suitable operating conditions were selected. More information about flow regimes and flow regime maps can be found in Zhang and Tang[22] and Link et al.[15] To obtain a comprehensive flow regime map for the 3D spout-fluid bed, pressure drop fluctuations were measured over a wide range of operating conditions. The background velocity was varied from 0 to 3.5 m/s with increments of 0.5 m/s and the spout velocity was varied from 40 to 95 m/s with increments of 5 m/s. Because of limitations of the setup, it was not possible to use spout velocities below 40 m/s. Consequently, the only spout velocity that was used below 40 m/s was 0 m/s.

Figure 3 shows the flow regime map that was recorded for the system under investigation. The operating conditions that were selected are marked in the flow regime maps and presented in Table 2, along with the details of the experiments and simulations. The background fluidization velocity exceeded the minimum fluidization velocity for all cases to avoid stagnant areas, which cannot be simulated efficiently with the hard sphere DPM.

All simulations were carried out on a computational grid consisting of 21 × 14 × 100 cells (width × depth × height).

Results

In this section, the spectral analyses of measured and computed pressure drop fluctuations will be presented, along with computed isosurface solids volume fraction plots and computed and measured particle velocity profiles.

The measured pressure drop fluctuations, which reflect the dynamic behavior of the bed, are used for both model validation, and to check for similar behavior in the separate experiments conducted at the two universities.

During the experiments, the pressure drop was recorded at a frequency of 100 Hz during periods of about 1 min and 1 h, at the University of Twente in The Netherlands (NL) and at the University of Birmingham in the United Kingdom (UK), respectively. The exact periods can be found in Table 2. In the numerical simulations, the computed pressure drop fluctuations were recorded at a frequency of 1000 Hz for a period of 20 s. Note that in the latter case, the first 3 s of the simulations were excluded from the spectral analysis to prevent start-up effects from influencing the results.

The amplitude of the pressure drop fluctuations is represented in terms of the root mean square (RMS) and is given in Table 3.

Table 3. Root Mean Square of the Measured and Computed Pressure Drop Fluctuations (Pa)

Case	B1	B2	B3
Experiment-NL	209	166	795
Experiment-UK	241	84	763
Simulation	226	34	463

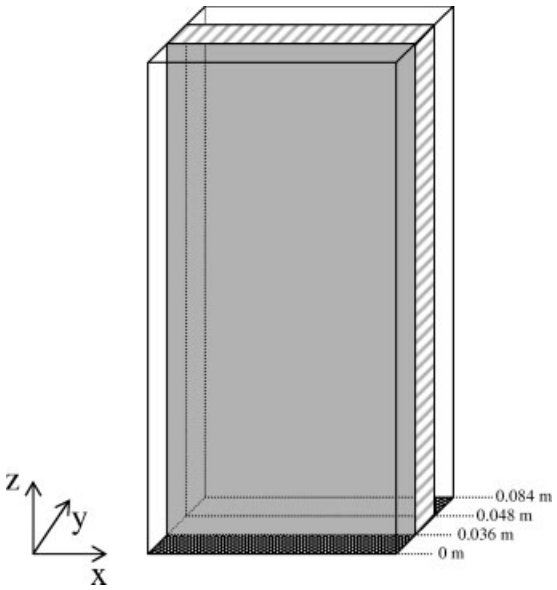

Figure 4. Schematic representation of central *xz*-plane in the geometry of the 3D bed.

To illustrate the behavior of the various flow regimes observed in a spout-fluid bed, and its relation to the pressure drop fluctuations, the computed bubble behavior is visualized using solids volume fraction isosurface plots at a solids volume fraction of 0.3. This value is used, because it is halfway between the solids volume fraction for the dense (~0.6) and dilute areas (~0.0).

The particle velocities resulting from the PEPT measurements are used to validate the more detailed aspects of the model results. The results of the PEPT measurements consisted of a particle trajectory from which a particle velocity history was derived. Consequently, for each time step the particle velocity was only known at a single location. To obtain a time-averaged velocity field the results from a measurement over a longer period of time were combined. Because information about the particle velocity in a certain

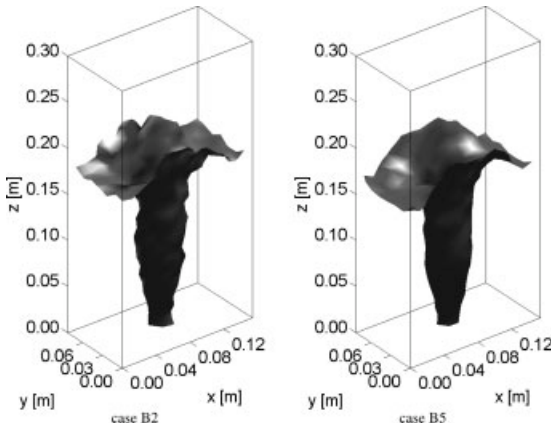

Figure 5. Plot of the simulated isosurface at a solids volume fraction of 0.3 for case B2, the spouting-with-aeration regime.

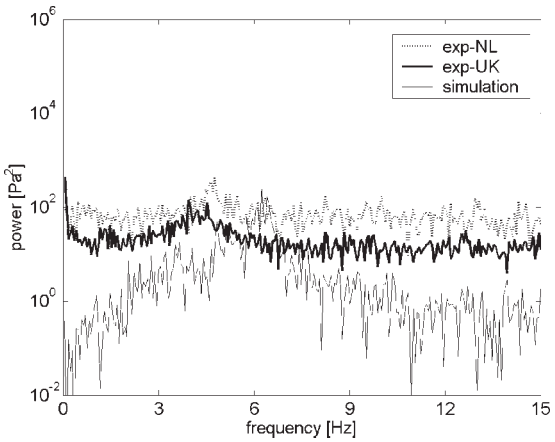

Figure 6. Frequency spectra of the measured and computed pressure drop fluctuations of case B2, the spouting-with-aeration regime.

area, or cell, can only be obtained when a particle is present, the time-average was obtained by averaging all particle velocities that were obtained within each cell:

$$\langle \mathbf{v}_{\mathrm{i,j,k}} \rangle = \frac{\sum_{i=1}^{N_t} \mathbf{v}_p \delta}{\sum_{i=1}^{N_t} \delta}, \quad \text{where} \begin{cases} \delta = 1 & \forall p \in i,j,k \\ \delta = 0 & \forall p \notin i,j,k \end{cases} \tag{10}$$

where p represents a particle in cell i, j, k and N_t is the number of time steps.

The measured and computed time-averaged particle velocities are presented through several types of charts. The overall flow field is represented by the particle velocity field in

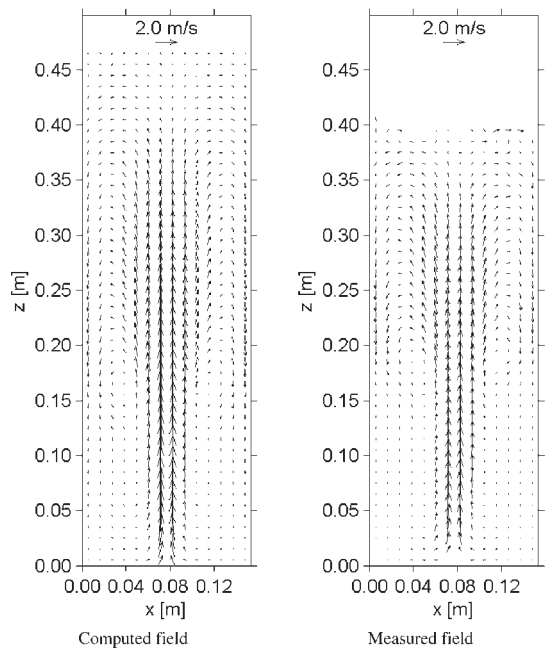

Figure 7. Time-averaged particle velocity fields in the central *xz*-plane for case B2, the spouting-with-aeration regime.

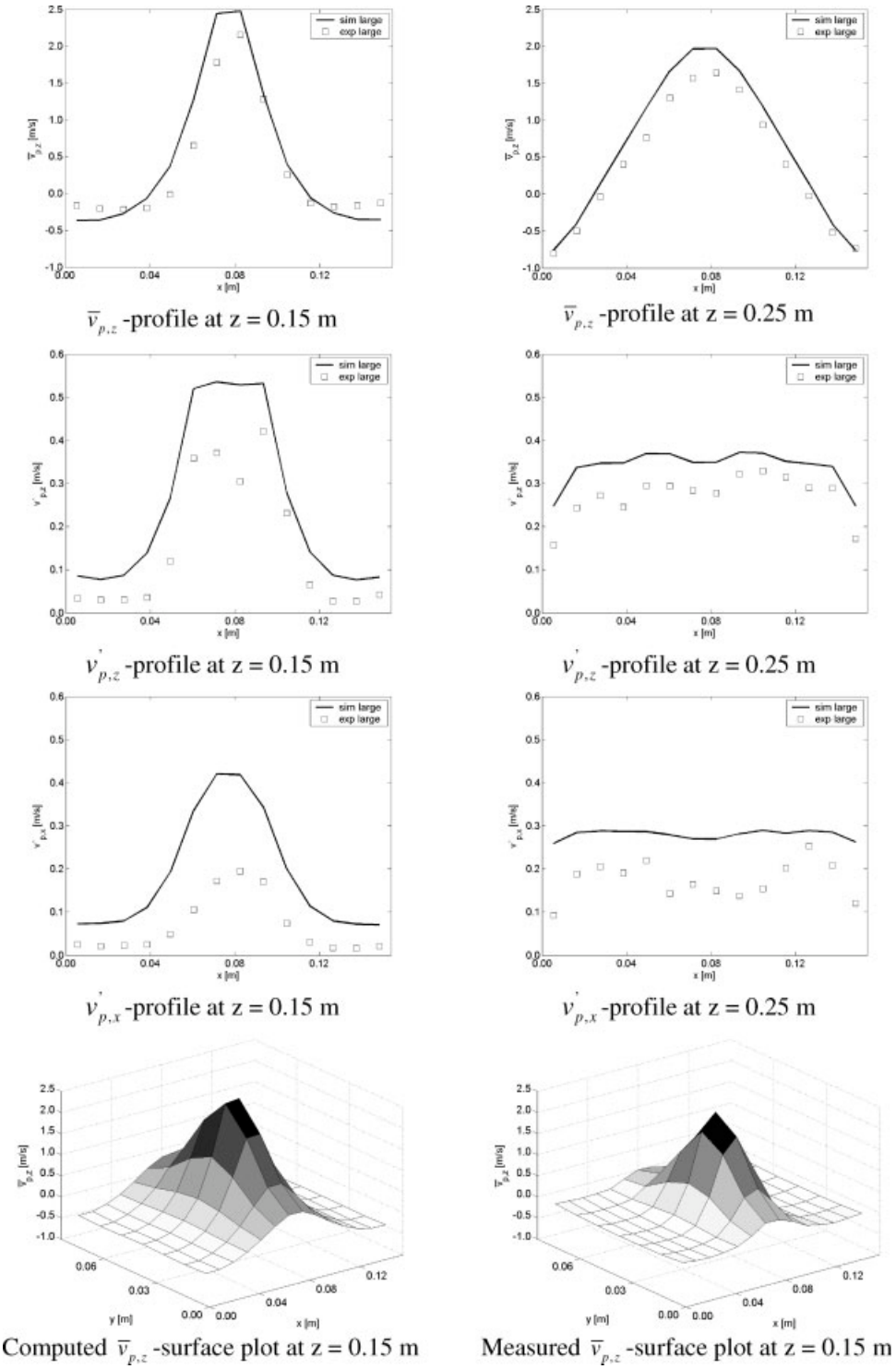

Figure 8. Profiles of the time-averaged vertical particle velocity including the RMS in the central *xz*-plane and a surface plot at $z = 0.15$ m for case B2, the spouting-with-aeration regime.

the central *xz*-plane, i.e., $0.036 < y \leq 0.048$ m, which is illustrated in Figure 4. Two particle velocity profiles in the central *xz*-plane are shown; one to illustrate the particle velocities in the annulus and the spout channel, at $z = 0.15$ m, and another to illustrate the particle velocities in the fountain, at $z = 0.25$ m. At these same levels a profile of the RMS of the particle velocity in both the horizontal ($v'_{p,x}$) and vertical ($v'_{p,z}$) direction is displayed. Finally, a surface plot of the velocity field in the *xy*-plane at $z = 0.15$ m is presented.

Spouting-with-aeration regime

In the spouting-with-aeration regime, the spout channel is stable and continuously penetrates the entire bed as can be

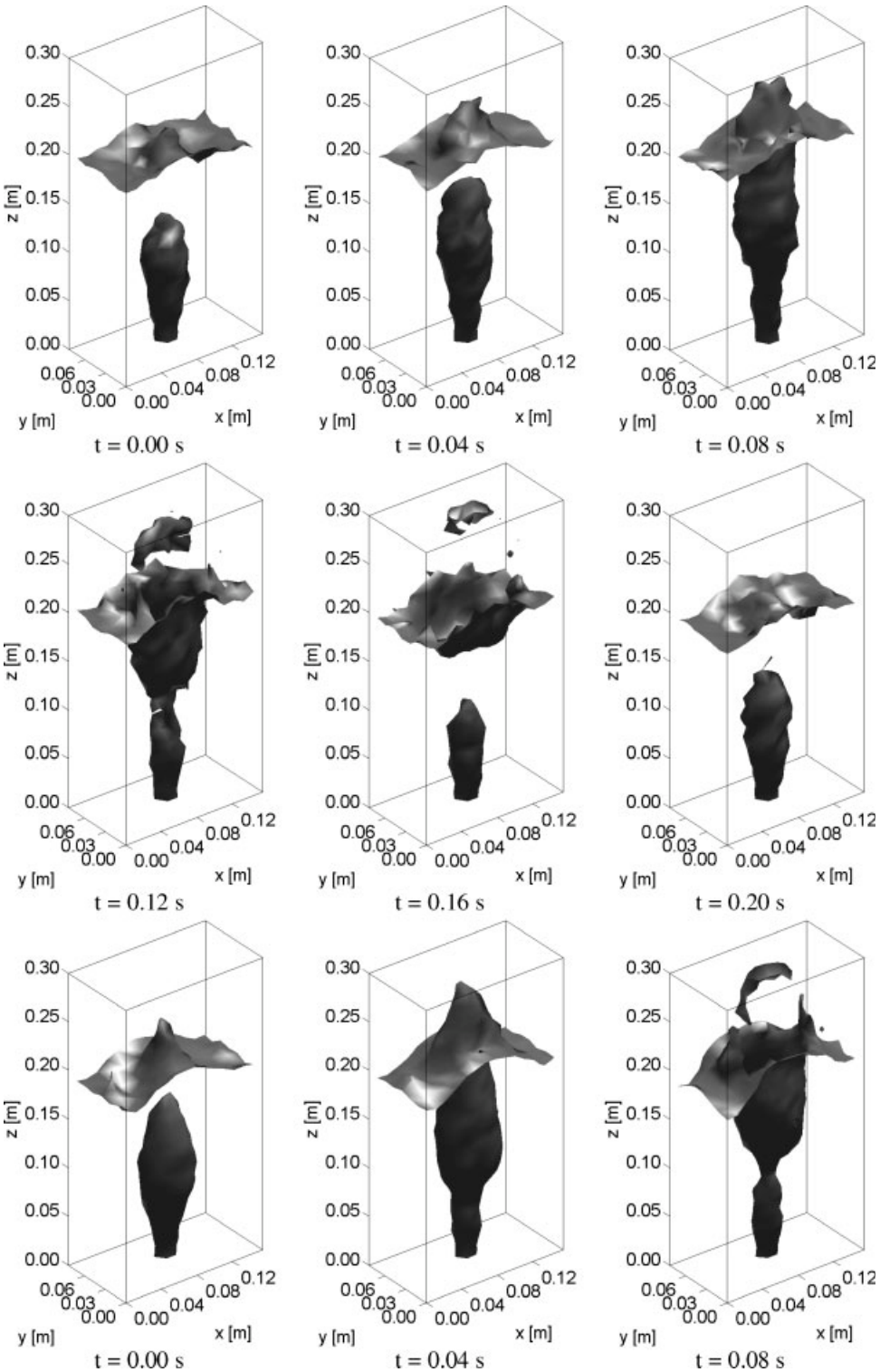

Figure 9. Plots of the simulated isosurface at a solids volume fraction of 0.3 for case B1, the intermediate/spout-fluidization regime.

seen in the solids volume fraction isosurface plots for case B2, which is presented in Figure 5.

As there is a continuous spout, the particle configuration itself does not change significantly, so the movement of the particles hardly affects the bed pressure drop. Consequently, the frequency spectra of the measured and computed pressure drop fluctuations, which are given in Figure 6, do not contain any significant peaks. The computed spectrum does however display a broad peak with very low power ($\sim$100 Pa^2) at a relatively high frequency (6 Hz, respectively, 7 Hz), which

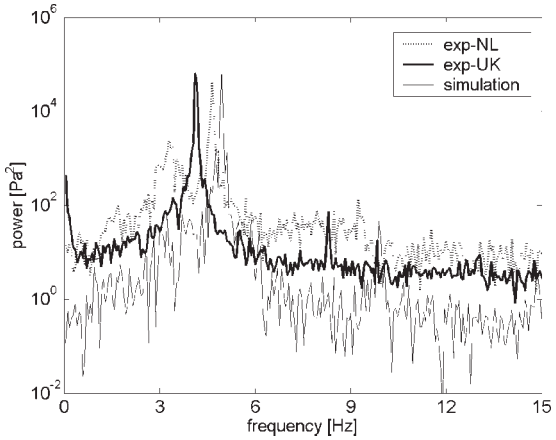

Figure 10. Frequency spectra of the measured and computed pressure drop fluctuations of case B1, the intermediate/spout-fluidization regime.

corresponds to an intermediate regime. Because the power is very small, the flow regime is much closer to the spouting-with-aeration regime than to the spout-fluidization regime. Apart from the broad peak, the trends in the frequency spectra are similar. Table 3 shows that the amplitude of the pressure drop fluctuations predicted by the DPM is considerably smaller than the measured value, although it is noted that both amplitudes are very small compared with the other cases. The magnitude of the maximum power of the pressure drop fluctuations, however, is comparable, which indicates that the pressure drop fluctuations predicted by the model were a little more regular.

Figures 7 and 8 show that the spouting-with-aeration regime displays a narrow spout channel with high time-averaged particle velocities due to the high gas velocity.

The profiles at a height of 0.15 m show that the RMS and the time-average of the particle velocities in the annulus are very small, which corresponds to the slow but continuous movement of the particles through the annulus toward the spout channel, which occurs in the spouting-with-aeration regime (see Figure 11). The RMS in the spout channel is much larger. Its value in the z-direction is approximately constant over the entire width of the channel. The RMS in the fountain is comparable with the RMS in the spout channel and approximately constant over the entire width of the bed.

The particle velocity fields displayed in Figure 9 show that the particles are projected less high into the freeboard in the measured case than in the computed case. Furthermore, the measured field shows no velocities in the bottom part of the spout channel. Despite these differences, the overall flow pattern is the same in both the measured and the computed result. The plots at $z = 0.15$ m displayed in Figure 11 illustrate that the region with upward flow is much larger in the simulation, although the shape of the profile is quite similar. Furthermore, the downward velocity is much more homogeneous in the experimental result. Additionally, the RMS is much larger in the computed result, while the shape of its profile is quite similar. The computed results are much closer to the measured results at $z = 0.25$ m. A comparison between the velocity fields and the isosurface plots shows that the positive vertical velocities generally occur in the dilute regions of the bed.

Spout-fluidization regime

In the spout-fluidization regime, an intermittent spout channel is present, which is periodically blocked by particles from the annulus. This behavior can be observed in the series of solids volume fraction isosurface plots for the case operating in the intermediate/spout-fluidization regime (case B1), which is shown in Figure 9. The plot illustrates how the spout channel grows in the vertical direction until it reaches the bed surface. Subsequently, a fountain is formed and the spout channel is closed halfway. The bottom half of the spout channel will then form the next bubble. It takes ~0.2 s to complete one cycle, which corresponds to a frequency of ~5 Hz.

The same frequency can also be observed in the frequency spectrum of the computed pressure drop fluctuations given in Figure 10. The frequency spectrum displays a narrow peak with large power ($\sim 1 \times 10^5$ Pa^2) at a relatively high frequency (4–6 Hz), which is representative of the spout-fluidization regime.[15] The trends in the frequency spectrum are very similar, although the model predicts the largest power at a higher frequency. Table 3 shows that the amplitude of the pressure drop fluctuations predicted by the simulations is in good agreement with the measured value, as is the magnitude of the power.

For case B1, the frequency spectra resulting from the measured UK and NL pressure drop fluctuations reveal some differences. To be able to compare the results, the frequency spectrum for the UK results is displayed, along with the

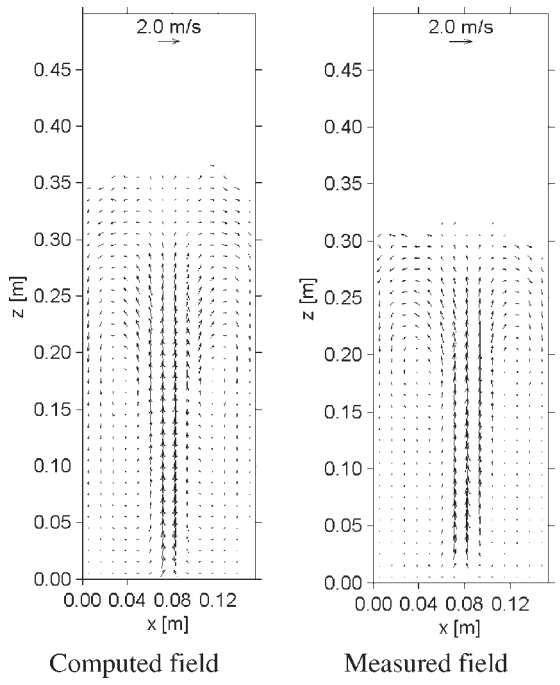

Figure 11. Time-averaged particle velocity fields in the central *xz*-plane for case B1, the intermediate/spout-fluidization regime.

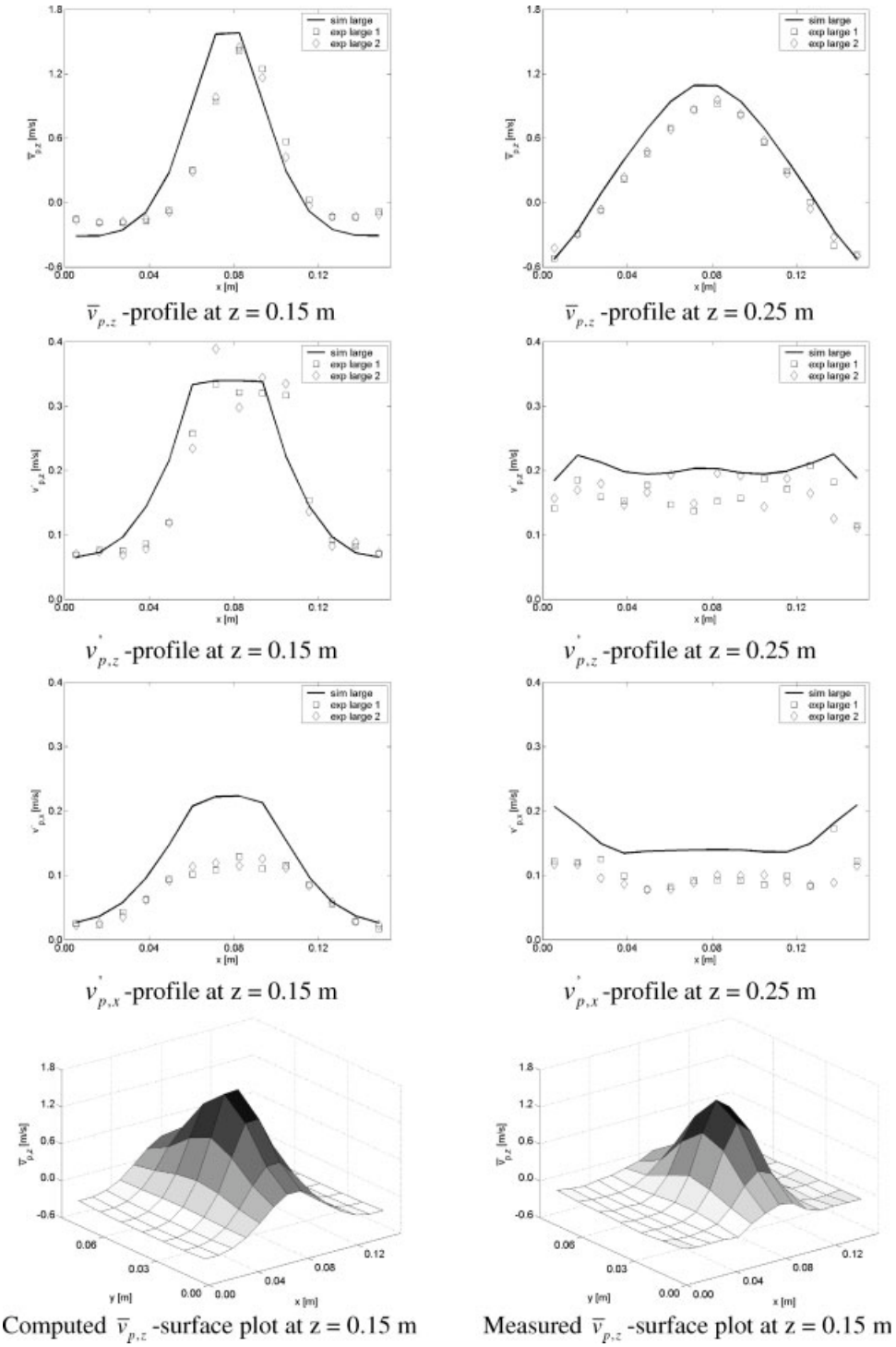

Figure 12. Profiles of the time-averaged vertical particle velocity including the RMS in the central *xz*-plane and a surface plot at $z = 0.15$ m for case B1, the intermediate/spout-fluidization regime.

results for the NL operating conditions closest to the UK operating condition. These frequency spectra show that the flow regime shifts from the spout-fluidization regime at a background velocity of 1.5 m/s to the intermediate regime at 2.0 m/s.

Consequently, a transition of the flow regime occurs between 1.5 and 2.0 m/s, which will most probably result in a less profound frequency peak compared with the extremely regular spout-fluidization regime. This can be observed in the measured UK frequency spectrum, which shows a reduced magnitude of the power.

Figures 11 and 12 show that the spout-fluidization regime displays a narrow spout channel with high time-averaged particle velocities due to the high gas velocity. Compared with

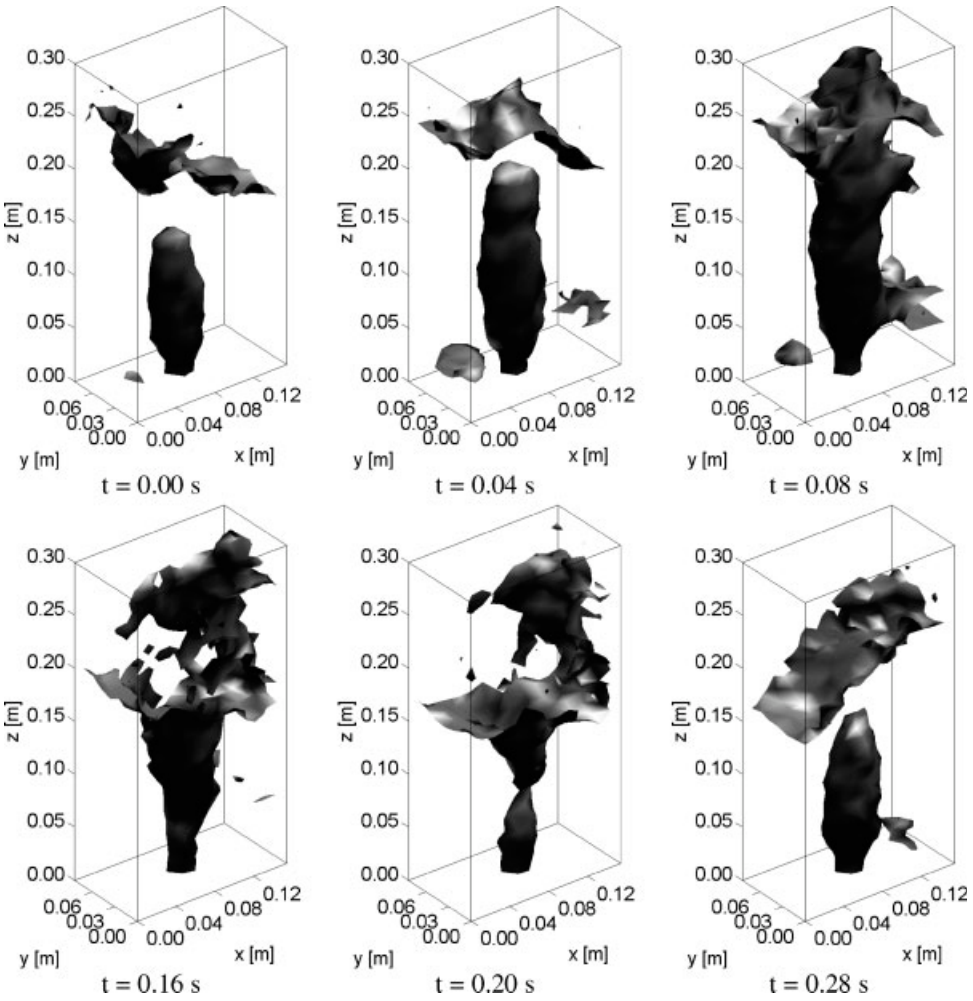

Figure 13. Plots of the simulated isosurface at a solids volume fraction of 0.3 for case B3, the jet-in-fluidized-bed regime.

the spouting-with-aeration regime this channel is somewhat wider.

The profiles at a height of 0.15 m show that the RMS and the time-average of the particle velocities in the annulus are rather small. The RMS is however considerably larger than the observed in the spouting-with-aeration regime, indicating that the particles in the annulus have more opportunity for random movement. In the spout channel the RMS and the time-average of the particle velocities are considerably smaller than in the spouting-with-aeration regime. The RMS in the z-direction is still approximately constant over the entire width of the channel. The RMS in the fountain is comparable with the RMS in the spout channel and approximately constant over the entire width of the bed.

The particle velocity fields show that the particles are projected less high into the freeboard in the measured case than in the computed case. Furthermore, the measured field shows smaller velocities in the bottom part of the spout channel. The measured velocity map shows a small artifact in the freeboard, which is related to the low number of samples in this region. Despite these differences, the overall flow pattern is quantitatively the same in both the measured and the computed result.

The plots at $z = 0.15$ m show that the region with upward flow is much larger in the simulation, although the shape of the profile is quite similar. Furthermore, the downward

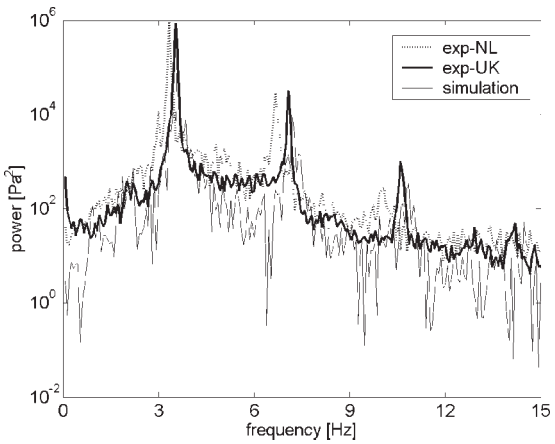

Figure 14. Frequency spectra of the measured and computed pressure drop fluctuations of case B3, the jet-in-fluidized-bed regime.

velocity is much more homogeneous in the experimental result. Additionally, the RMS is much larger in the computed result, while the shape of its profile is quite similar. The computed results are much closer to the measured results at $z = 0.25$ m.

Jet-in-fluidized-bed regime

In the jet-in-fluidized-bed regime, the bed contains both a spout channel and bubbles that are interacting with one another, which is illustrated by the solids volume fraction isosurface plots for the case in the jet-in-fluidized-bed regime (B3), displayed in Figure 13. This figure shows a spout channel that grows in the vertical direction until it reaches the bed surface, while small bubbles are present in the annulus, which merge with the spout channel. Subsequently, a fountain is formed and the spout channel is closed halfway up. Finally, a new bubble is formed in the lower half of the spout channel.

This process consumes ~0.3 s, which corresponds to the frequency of ~3.5 Hz, which can be observed in the frequency spectra of the computed pressure drop fluctuations given in Figure 14. The frequency spectra of the measured and computed pressure drop fluctuations are in very good agreement. Both display a relatively narrow peak with very large power ($\gg 1 \times 10^5$ Pa^2) at an intermediate frequency (~3.5 Hz), which is typical for the single frequency mode of this flow regime. The frequency spectra resulting from the measured UK and NL pressure drop fluctuations are comparable.

Table 3 shows that the amplitude of the pressure drop fluctuations predicted by the DPM is considerably smaller (40%) than the measured value, which results in a lower magnitude of the power of the pressure drop fluctuations.

Figures 15 and 16 show that the single frequency mode of the jet-in-fluidized-bed regime displays a narrow spout channel with high time-averaged particle velocities due to the high gas velocity.

The profiles at a height of 0.15 m show that the time-average of the particle velocities in the annulus is rather small. The RMS is however only slightly smaller than in the spout channel and considerably larger than that observed in the spout-fluidization regime, indicating that the particles in the annulus have much more opportunity for random movement. In the spout channel the RMS and the time-average of the particle velocities are comparable to the spout-fluidization regime. The RMS in the fountain is comparable with the RMS in the spout channel and approximately constant over the entire width of the bed.

Discussion

Frequency spectra

Based on the good agreement in the frequency spectra, it is concluded that the model was able to predict the appropriate flow regime in most cases. Furthermore, the amplitude of the pressure drop fluctuations predicted by the model was of the same order as the experimental result, although some differences were observed. The frequency at which the largest power was found was generally overpredicted by the model. For a number of cases, the fluctuations predicted by the model were more regular than the measured fluctuations. When the predictive capabilities of the model are evaluated, it can be concluded that the model accurately predicts the flow regimes.

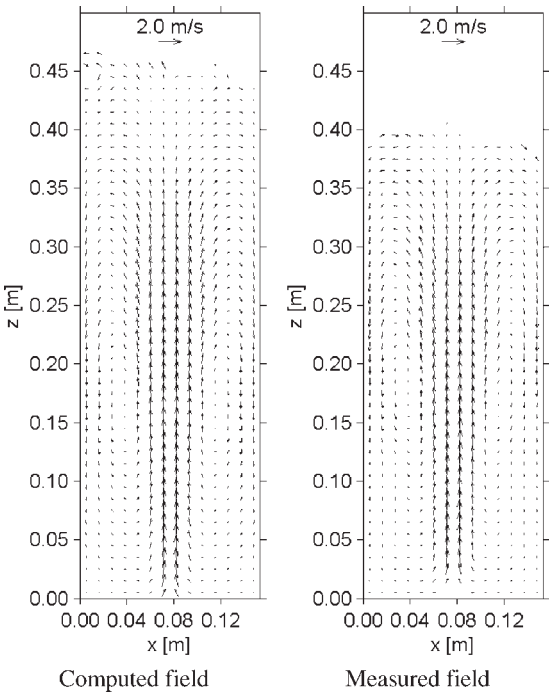

Figure 15. Time-averaged particle velocity fields in the central *xz*-plane for case B3, the jet-in-fluidized-bed regime.

The differences that were observed between the measured and simulated bed behavior can in principle be attributed to the representation of gas–particle and/or particle–particle interaction. A sensitivity study with respect to the values of the collision parameters for both particle–particle and particle–wall interaction revealed that the observed differences could not be reduced significantly by using different values for these parameters.[17] This leaves the representation of the fluid–particle interaction as a probable cause for most of the observed discrepancies. Although the fluid–particle drag obtained from lattice Boltzmann simulations is believed to be reasonably accurate, it is obtained for systems in which the particles are homogeneously distributed in space. Heterogeneity in void fraction is known to exist in dense gas–particle flows, especially around gas bubbles. The effect of this heterogeneity on effective fluid–particle drag is largely unexplored, but it can in principle be resolved from detailed lattice Boltzmann simulations.

Particle velocities

The measured and computed time-averaged particle velocity fields generally display good agreement. The particle flow patterns are very similar, although the simulations show particles being projected higher into the freeboard. This may be a statistical issue, because the total amount of data collected

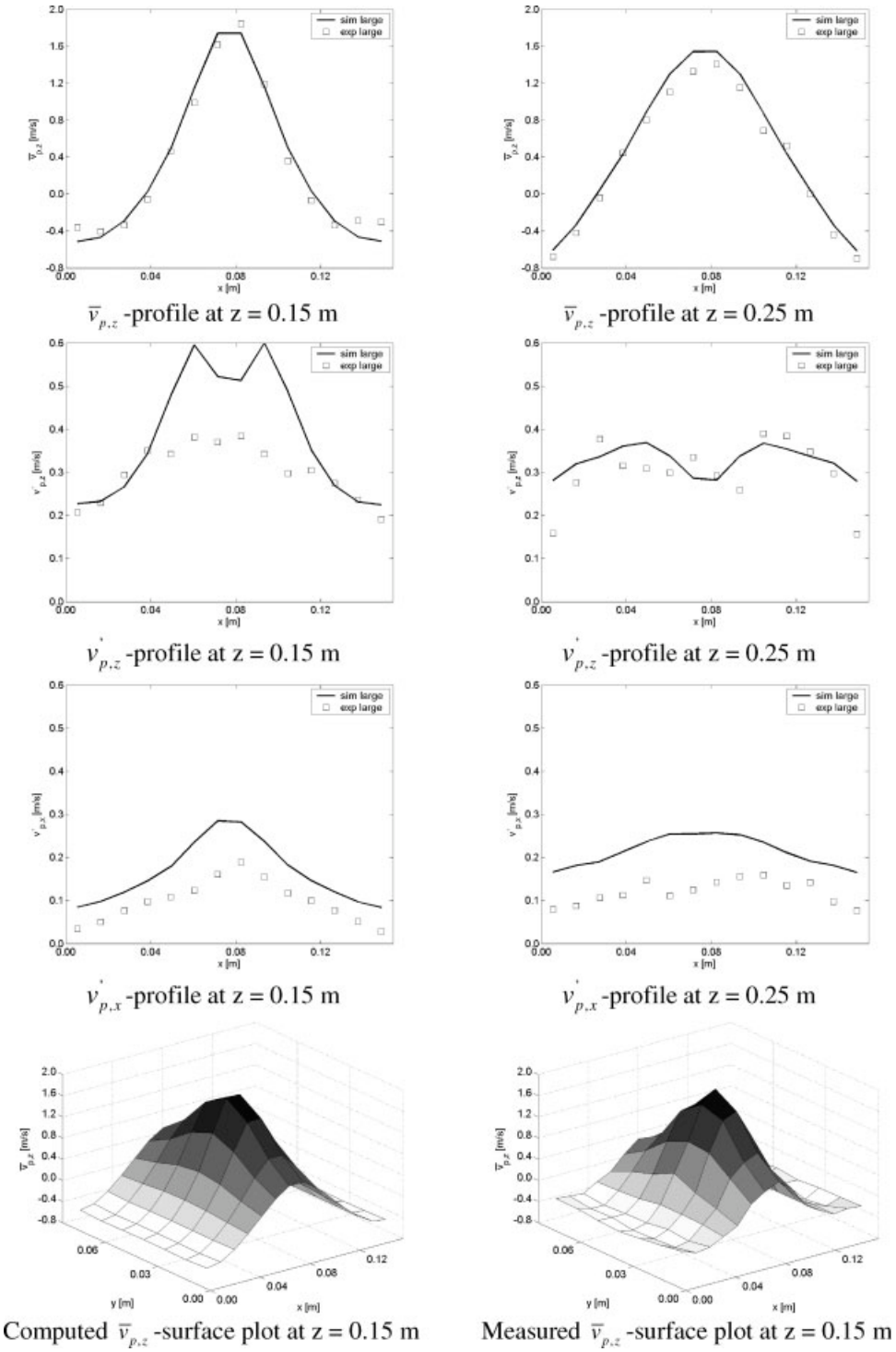

Figure 16. Profiles of the time-averaged vertical particle velocity including the RMS in the central *xz*-plane and a surface plot at $z = 0.15$ m for case B3, the jet-in-fluidized-bed regime.

using PEPT (1 h/particle × 1 particle ~ 1 h) is rather less than the total amount of data obtained from the simulation [16 s/particle × (4.5×10^4) particles ~ 200 h]. It is also the case that very rapid accelerations can result in underestimation of velocities measured using PEPT, because of the six-point velocity determination method usually employed.

The measured and computed particle velocity profiles show good agreement. At a height of 0.15 m, the shape of the computed profile differs slightly from the measured profile in all cases. The simulations show positive velocities in large regions of the bed, which is compensated by more negative velocities close to the wall. At a height of 0.25 m, the

agreement is very good, except for case B1, the intermediate/spout-fluidization regime, and B2, the spouting-with-aeration regime, where the particle velocity in the center of the bed is slightly overpredicted by the model.

The particle velocity field at $z = 0.15$ m shows that the velocity peak in the center of the bed is generally narrower in the experiments. This necessarily leads to a lower than predicted downward velocity in the downflowing regions.

Conclusions

In this article, the capability of the DPM was assessed to reproduce several of the important flow regimes observed in a 3D spout-fluid bed. For all cases, the model successfully predicted the flow regime, although some (small) differences with the experimental results were observed. In most cases, the frequency, at which the largest power is found is overpredicted by the model. Furthermore, the fluctuations predicted by the model are generally more regular than the measured fluctuations.

The remaining differences between the computed and experimentally observed bed behavior are most probably related to the representation of the effective fluid–particle interaction in the DPM, which relies on a homogeneous distribution of the particles on the length scale that is used to calculate the fluid–particle drag. The effect of heterogeneity on the fluid–particle interaction, which arises, for example, around gas bubbles, should be investigated. Lattice Boltzmann simulations would be well suited for this purpose.

The particle velocity for a monodisperse system was investigated with the use of the model and PEPT. The computed results were compared with velocity maps determined from particle trajectories acquired using PEPT.

The DPM accurately reproduces measured time-averaged particle velocities for all investigated conditions and is therefore able to capture the details of the particle flow in various flow regimes. Plots of the particle velocity in the z-direction in a cross section of the column do however show that the width of the spout channel, i.e. the region where upward particle velocities are encountered, is larger in the simulations. At the border between the spout channel and the annulus, the same type of heterogeneity in the solids volume fraction is present, which was already described in the discussion of the results for the pressure drop fluctuations. This supports the recommendation to study the effect of heterogeneity on the fluid–particle drag in more detail.

The computed RMS of the particle velocity was in reasonable agreement with the measured values, especially when the various disturbances present in the experiments are taken into account.

The RMS of the particle velocities in the vertical direction is about twice as large as that in the horizontal direction.

Overall, the model predicts the correct dynamics and quantitative particle velocities in a spout-fluid bed. There is however still room for improvement, especially regarding the treatment of the drag force at the boundary between dense and dilute areas around bubbles. Nevertheless, these results confirm the suitability of the DPM to study processes involving spout-fluid beds. This enables detailed studies of systems that are difficult if not impossible to study experimentally, such as the growth rate of each individual particle as a function of its location in a spout-fluid bed granulator.

Notation

d = diameter, m
D = distribution function
e_n = coefficient of normal restitution
$\mathbf{g}$ = gravitational acceleration, m/s^2
$\mathbf{I}$ = unit vector
m_p = particle mass, kg
N_t = number of time steps
p = pressure, Pa
$\mathbf{r}$ = position, m
Re_p = particle Reynolds number
$\mathbf{S}_p$ = particle drag sink term, N/m^3
t = time, s
$\mathbf{u}$ = gas velocity, m/s
$\mathbf{v}_p$ = particle velocity, m/s
V = volume, m^3

Abbreviations

3D = three-dimensional
DPM = discrete particle model
NL = at the University of Twente in The Netherlands
PEPT = positron emission particle tracking
RMS = root mean square
UK = at the University of Birmingham in the United Kingdom

Greek letters

β = interphase momentum transfer coefficient, kg/(m^3 s)
β_0 = coefficient of tangential restitution
ε = volume fraction
λ_f = gas phase bulk viscosity, kg/(m s)
μ_f = gas phase shear viscosity, kg/(m s)
μ = dynamic friction coefficient
ρ = density, kg/m^3
τ_f = gas phase stress tensor, Pa
Φ = particle flux, kg/(m^2 s)

Subscripts

bg = background fluidization
exp = experimental
f = fluid phase
mf = minimum fluidization
p = particle
pdf = pressure drop fluctuations
sim = simulation
sp = spout fluidization
sup = superficial
w = wall
x = horizontal direction
z = vertical direction

Acknowledgments

The authors thank Senter and Yara Sluiskil, The Netherlands, for their financial support to the project. J. Wood thanks the British Council-NWO for funding under the Partnership Program in Science to visit the University of Twente in The Netherlands.

Literature Cited

1. Littman H, Morgan MH III, Narayanan PV, Kim SJ, Day J-Y. An axisymmetric model of flow in the annulus of a spouted bed of coarse particles: model, experimental verification and residence time distribution. *Can J Chem Eng*. 1985;63:188–194.

2. Kawaguchi T, Sakamoto M, Tanaka T, Tsuji Y. Quasi-three-dimensional numerical simulation of spouted beds in cylinder. *Powder Technol*. 2000;109:3–12.
3. Link JM, Zeilstra C, Deen NG, Kuipers JAM. Validation of a discrete particle model in a 2D spout-fluid bed using non-intrusive optical measuring techniques. *Can J Chem Eng*. 2004;82:30–36.
4. Seville JPK, Ingram A, Parker DJ. Probing Processes Using Positrons. *Chem Eng Res Des*. 2005;83:788–793.
5. Stein M, Martin TW, Seville JPK, McNeil PA, Parker DJ. Positron emission particle tracking: particle velocities in gas fluidised beds, mixers and other applications. In: Chaouki J, Larachi F, Dudukovic MP, editors. *Non Invasive Monitoring of Multiphase Flows*. Amsterdam: Elsevier, 1997:161–184.
6. Stein M, Ding YL, Seville JPK, Parker DJ. Solids motion in bubbling gas fluidised beds. *Chem Eng Sci*. 2000;55:5291–5300.
7. Hoomans BPB, Kuipers JAM, Mohd Salleh MA, Stein M, Seville JPK. Experimental validation of granular dynamics simulations of gas-fluidised beds with homogeneous in-flow conditions using Positron Emission Particle Tracking. *Powder Technol*. 2001;116:166–177.
8. Larachi F, Chaouki J, Kennedy G. 3-D mapping of solids flow fields in multiphase reactors with RPT. *AIChE J*. 1995;41:439–443.
9. Moslemian D, Devanathan N, Dudukovic MP. Radioactive particle tracking technique for investigation of phase recirculation and turbulence in multiphase systems. *Rev Sci Instrum*. 1992;63:4361–4372.
10. Westerweel J. Fundamentals of digital particle image velocimetry. *Meas Sci Technol*. 1997;8:1379–1392.
11. Takeuchi S, Wang XS, Rhodes MJ. Discrete element study of particle circulation in a 3-D spouted bed. *Chem Eng Sci*. 2005;60:1267–1276.
12. Takeuchi S, Wang S, Rhodes M. Discrete element simulation of a flat-bottomed spouted bed in the 3-D cylindrical coordinate system. *Chem Eng Sci*. 2004;59:3495–3504.
13. Swasdisevi T, Tanthapanichakoon W, Charinpanitkul T, Kawaguchi T, Tanaka T, Tsuji Y. Investigation of fluid and coarse-particle dynamics in a two-dimensional spouted bed. *Chem Eng Technol*. 2004;27:971–981.
14. Zhong W, Xiong Y, Yuan Z, Zhang M. DEM simulation of gas-solid flow behaviors in spout-fluid bed. *Chem Eng Sci*. 2006;61:1571–1584.
15. Link JM, Cuypers LA, Deen NG, Kuipers JAM. Flow regimes in a spout-fluid bed: a combined experimental and simulation study. *Chem Eng Sci*. 2005;60:3425–3442.
16. Hoomans BPB, Kuipers JAM, Briels WJ, Van Swaaij WPM. Discrete particle simulation of bubble and slug formation in a two-dimensional gas-fluidised bed: a hard-sphere approach. *Chem Eng Sci*. 1996;51:99–118.
17. Link JM. Development and validation of a discrete particle model of a spout-fluid bed granulator. PhD Thesis, University of Twente, Enschede, 2006.
18. Goldschmidt MJV, Kuipers JAM, Van Swaaij WPM. Hydrodynamic modeling of dense gas-fluidised beds using the kinetic theory of granular flow: effect of coefficient of restitution on bed dynamics. *Chem Eng Sci*. 2001;56:571–578.
19. Kharaz AH, Gorham DA, Salman AD. Accurate measurement of particle impact parameters. *Meas Sci Technol*. 1999;10:31–35.
20. Koch DL, Hill RJ. Inertial effects in suspension and porous-media flows. *Annu Rev Fluid Mech*. 2001;33:619–647.
21. Bird RB, Stewart WE, Lightfoot EN. *Transport Phenomena*. New York: Wiley, 1960:79.
22. Zhang J-Y, Tang F. Classification and determination of flow regimes in spout-fluidized beds. In: Proceedings of the 11th International Conference on Fluidization, Naples, Italy, May 9–14, 2004:491–498.

Manuscript received Feb. 23, 2007, and revision received Dec. 19, 2007.